Cranfield UNIVERSITY

SCHOOL OF AEROSPACE,TRANSPORT AND MANUFACTURING

Numerical methods for Compressible Flows

Giorgio SOGGIU, s318801

Word count:4052 (count by Latex editor)

June 3, 2023

Abstract

Three case study experiments are used to identify compare the merits of fluxes and limiters. HLL, HLLC, Rusanov, Lax-Friedrich fluxes associated to Barth & Jespersen and Venkatakrishnan limiters are put in competition. The Cylindrical Explosion, The Forward facing step and the Double mach reflection generate interesting flow features. HLLC gives better results for the Cylindrical Explosion and The Forward facing step. A fifth order WENO is particularly conclusive in The Double mach reflection. Distinguishing limiters' influence is complex.

keywords: Forward facing step, Double mach reflection, Cylindrical explosion, Rusanov Flux, HLLC, Bart Jespersen limiter, Venkatakrishnan limiter, Godunov, finite element method, shock waves, contact discontinuities, rarefaction wave

Contents

List of Figures

List of Tables

1 List of Abbreviations

LXF	Lax-Friedrich Flux
1D	1 dimension
2D	2 dimensions

Table 1: abbreviations

2 Introduction

Shocks, contact discontinuities and complex structures which arise in simulations of compressible gas dynamics lead to difficulties when Computing them[6]. Different methods have been developed to capture these phenomena. Case study experiments exist to challenge and identify the merit of each method. In the current study computations are produced over three experiments; The Cylindrical Explosion (1 dimension and 2 dimensions), The Forward Facing step and the Double Mach reflection[6]. The motivation of the work is to validate code implementation by comparing obtained results to given Reference data and phenomena depicted by Woodward & Colella and Gary A.SOD. In a second time, computation's accuracy are put in competition to identify, for each experiment, the scheme and limiters which gives the most conclusive results.

Experiments, Presentation

The Cylindrical Explosion experiment is conducted in 1 and 2 dimensions. The experiments divide a shock tube in two regions of different gas parameters[6]. In both regions parameters are constant. A cylinder of radius 0.4 makes the separation. The density and pressure are given respectively for 1 and 2D by;

1D:

$$(\rho, p) = \begin{cases} (1.0, 1.0), & r \leq 0.4, \\ (\rho_0, p_0), & r > 0.4, \end{cases} \tag{1}$$

$$u = v = 0, \ r^2 = x^2. \tag{2}$$

2D:

$$(\rho, p) = \begin{cases} (1.0, 1.0), & r \leq 0.4, \\ (\rho_0, p_0), & r > 0.4, \end{cases} \tag{3}$$

$$u = v = 0, \ r^2 = x^2 + y^2. \tag{4}$$

Forward facing step The case study experiment of the Forward facing step has been introduced by Emery and has proved itself in the field. The tunnel is initially filled with a gamma-law gas with $\gamma = 1.4$ having a density 1.4, a pressure of 1 and a velocity of 3. Reflecting boundary conditions are applied on the walls of the tunnel[6]. A uniform Mach 3 flow moves inside the two-dimensions tunnel containing a step. The tunnel is 1 unit wide and 3 units long. The step is positioned 0.6 unit from the left-hand side of the tunnel and is 0.2 units high. Further details of the Experiment are provided in the original paper of Emery and the paper of Woodward & Colella[6].
The Experiment yields to the formation of interesting physical features, which, in the current assignment, are described in the 'Results and Discussions' section.

Double mach reflection A planar shocks strikes with an angle of 60 degrees the bottom wall of a two-dimensions tube[6]. This phenomena generates a reflective shock and additional features leading to a Double Mach reflection[6]. It generates steady and unsteady structures[6]. In the current study , the flow is characterized by a Mach number equals to 10. Ahead of the incident shock, the air is undisturbed

and has; a density of 1.4 and a pressure of 1. Parameters are similar to those used in the paper of Woodward & Collela[6]. Nota: this experiment is considered as a good evaluation for Euler codes [6].

These Experiments lead to apparitions of complex phenomena such as shocks and rarefaction waves or contact discontinuities. Their influence on physical features is highly studied in the field[6].

Types of Waves

Shocks

This origin of shock waves is linked to compression wave[4].Inside a compression wave, the flow decelerates,the pressure and temperature increase. New disturbances created travel faster than the previous one (because of pressure and temperature). The wave travelling behind catches up the first one and they collide[4]. A shock wave is created having an extremely large gradient of pressure, density and temperature. The velocity drastically decreases inside a shock wave. Properties' evolution inside a shock wave[4]:

- Mach number:decreases

- Static pressure:increases

- stagnation pressure:decreases

- static temperature:increases

- stagnation temperature: constant

- density:increases

- velocity:decreases

- entropy:increases

The stagnation pressure decreases as it requires energy to displace molecules across the shock wave.Hence, the fluid is loosing energy[4].

As the shock wave does not generate work and there is no heat addition, total enthalpy and total temperature remain constant[4]. There are different type of shocks: oblique and normal.

The Normal shock wave is at $90°$of the oncoming supersonic stream. It results in a subsonic state (the flow evolves from supersonic to subsonic conditions)[4].The Normal shock is depicted by some of the following equations:
-Rayleigh equation[4];

$$\frac{p_2}{p_1} = \frac{1 + \gamma M_1^2}{1 + \gamma M_2^2} \tag{5}$$

-Fanno equation[4];

$$\frac{p_2}{p_1} = \frac{M_1}{M^2}(\frac{2 + (\gamma - 1)M_1^2}{2 + (\gamma - 1)M_1^2})^{0.5} \tag{6}$$

-M2 can be isolated[4];

$$M_2^2 = \frac{(\gamma - 1)M_1^2 + 2}{2\gamma M_1^2 - (\gamma - 1)} \tag{7}$$

The Oblique shock can occur when the inflow is supersonic[4]. The outflow can be either subsonic, sonic or supersonic. An oblique shock is inclined to the inflow direction[4]. The Oblique shock is depicted by some of the following equations (which can be obtained from normal shock equations replacing: M1 by $M1sin(\beta)$ and M2 by $M2sin(\beta - \delta)$)[4]:

$$M_2^2 sin^2(\beta - \delta) = \frac{(\gamma - 1)M_1^2 sin^2(\beta) + 2}{2\gamma M_1^2 sin^2(\beta) - (\gamma - 1)} \tag{8}$$

$$\frac{T_2}{T_1} = (\frac{2\gamma M_1^2 sin^2(\beta) - (\gamma - 1)}{(\gamma + 1)})(\frac{2 + (\gamma - 1)M_1^2 sin^2(\beta)}{(\gamma + 1)M_1^2 sin^2(\beta)} \tag{9}$$

$$\frac{p_2}{p_1} = \frac{2\gamma M_1^2 sin^2(\beta) - (\gamma - 1)}{(\gamma + 1)} \tag{10}$$

$$\frac{\rho_2}{\rho_1} = \frac{u_1}{u_2} = \frac{(\gamma + 1)M_1^2 sin^2(\beta)}{(\gamma - 1)M_1^2 sin^2(\beta) + 2} \tag{11}$$

Rarefaction

In a rarefaction wave, the matter is rarefied. The density decreases. This transition from high density to lower density takes time (following the Hugoniot curve) and space[4]. After a shock wave, a rarefaction wave occurs.

Contact discontinuities

A contact discontinuity is a surface making a separation between two zones of different densities and temperature. At a contact discontinuity the pressure is constant and there are no gas flows across the surface[3].

Description Godunov, Riemann

The Euler equation is used to describe compressible matter for inviscid flows[3]. It is obtained neglecting viscous stresses, heat conduction and body forces[3]. The two-dimensions Euler equation in the conservative form stated with conservative variables is given by (compact notation)[3];

$$U_t + F(U)_x + G(U)_y = 0 \tag{12}$$

with $U = \begin{bmatrix} \rho \\ \rho u \\ \rho v \\ E \end{bmatrix}$, $F = \begin{bmatrix} \rho u \\ \rho u^2 + p \\ \rho uv \\ u(E + p) \end{bmatrix}$, $G = \begin{bmatrix} \rho v \\ \rho uv \\ \rho v^2 + p \\ v(E + p) \end{bmatrix}$

The Godunov methods calculates the fluxes at cells interfaces using the local solution of the local Riemann problem[3]. In the integral form of the Euler equation, Godunov method is expressed[3] as;

$$U_i^{n+1} = U_i^n - \frac{1}{\triangle x} \int_t^{t^{n+1}} (F_{i+\frac{1}{2}} - F_{i-\frac{1}{2}})dt \tag{13}$$

The conservative form of the Godunov method is given by

$$U_i^{n+1} = U_i^n + \frac{\triangle t}{\triangle x}[F_{i-\frac{1}{2}} - F_{i+\frac{1}{2}}] \tag{14}$$

Where $F_{i-\frac{1}{2}}$ and $F_{i+\frac{1}{2}}$ are the fluxes at the interfaces. They required $U_{i-\frac{1}{2}}$ and $U_{i+\frac{1}{2}}$, also called the exact similarity solution of the Riemann problem having initial state;

$$U(x,0) = \begin{Bmatrix} U_L & if & x < 0, \\ U_R & if & x > 0, \end{Bmatrix} \tag{15}$$

6

Initial state is constant for both positive and negative but differ between the right and left side.This phenomena is "naturally" visible in discretisation used for finite element methods which generate discontinuity/ies in cell interfaces[3]. Its impact is more important at shocks and contact discontinuities. To counteract the difficulties of computing them by iterative processes, Riemann solvers have been developed. These solvers must satisfy the CFL conditions considered as a necessary (not always sufficient) criteria for stability and convergence to the solution. The Riemann problem solution is built on a superposition of waves[3]. Snmax is the maximum wave speed of both right and left side of the intercell. Approximation of the functions $F_{i-\frac{1}{2}}$ and $F_{i-\frac{1}{2}}$ can be found directly by the use of Riemann solvers. Brief presentation of their fluxes is proposed in the following paragraph.

Lax-Friedrich FLux

$$F^{Rusanov} = \frac{1}{2}(F_L + F_R) - \frac{1}{2}S^+(U_R - U_L) \tag{16}$$

disadvantage;

- highly diffusive

The HLL Riemann Solver is given by;

$$U^{hll}(x,t) = \begin{cases} U_L \ \ if \ \ \frac{x}{t} \leq S_L, \\ U^{hll} \ \ if \ \ S_L \leq \frac{x}{t} \leq S_R, \\ U_R \ \ if \ \ \frac{x}{t} \geq S_R, \end{cases} \tag{17}$$

Where U^{hll} is the constant state vector. In the case of the HLL Riemann solver, the structure of the solution is depicted by two waves separating three states[3]. S_L and S_R are waves' speed. The corresponding HLL flux at cell interfaces is expressed as;

$$F_{i+\frac{1}{2}}^{hll} = \begin{cases} F_L \ \ if \ \ 0 \leq S_L, \\ F^{hll} = \frac{S_R F_L - S_L F_R + S_L S_R (U_R - U_L)}{S_R - S_L} \ \ if \ \ S_L \leq 0 \leq S_R, \\ F_R \ \ if \ \ 0 \geq S_R, \end{cases} \tag{18}$$

disadvantages:

- can't keep contact discontinuities sharp. It ignores the middle wave (the mass advection wave).

- approximates all waves as jumps (not every wave is a jump: in particular the expansion wave).

One of the main disadvantages of this HLL solver is that it cannot keep contact discontinuities sharp[3]. It adds numerical dissipation to flow features. This is not surprising since there is no middle wave in this scheme. Moreover the two-waves configuration is not adapted to large systems like the Euler equation[3]. To overcome these difficulties, HLLC solver has been created.

The HLLC Riemann Solver is given by;

$$U^{hllc}(x,t) = \begin{cases} U_L \ \ if \ \ \frac{x}{t} \leq S_L, \\ U^{*L} \ \ if \ \ S_L \leq \frac{x}{t} \leq S_*, \\ U^{*R} \ \ if \ \ S_* \leq \frac{x}{t} \leq S_R, \\ U_R \ \ if \ \ \frac{x}{t} \geq S_R, \end{cases} \tag{19}$$

It fluxes are given as follows;

$$F_{i+\frac{1}{2}}^{hllc} = \begin{cases} F_L \ \ if \ \ 0 \leq S_L \\ F_{*L} = F_L + S_L(U_{*L} - U_L) \ \ if \ \ S_L \leq 0 \leq S_* \\ F_{*R} = F_R + S_R(U_{*R} - U_R) \ \ if \ \ S_* \leq 0 \leq S_R \\ F_R \ \ if \ \ 0 \geq S_R \end{cases} \tag{20}$$

advantages[3]:

- contact and shear waves are repaired

Godunov methods, finite element methods, drawbacks

Godunov's method, drawbacks[3]

- the use of Riemann solver increases significantly the computational cost. The MacCormack scheme used in [6] requires two times less Computational element than first order Riemann solver.

- the elaborate calculations of the fluxes reduce the computing speed of the scheme

- has the tendency to emit noise. This phenomena is visible in the experiment "A Mach 3 Wind Tunnel with a step" from [6].

Finite element scheme,drawbacks[3]

- such scheme have numerical diffusion and dispersion. They are due to truncation error. Hence, diffusion on contact discontinuities increases as the calculation runs [7]

- According to Gary [7], finite element methods produce numerical oscillations when the problem implies discontinuities

Performance

Simulations have been performed on a computer with the following properties;

- Processor ; Intel(R) Core(TM) i7-4790 CPU@ 3.60 GHz 3.60GHz

- Installed RAM; 16.0 GB

3   Methods/Procedures

Three experiments are conducted. The Validation and Comparative study is performed qualitatively and quantitatively for the Cylindrical Explosion (1D). The qualitative study is based on first and second order fluxes on three meshes. The following features are studied: rho, u, P, T.

Consideration is put on the density. The quantitative study is performed on the finest mesh and uses second order fluxes. The quantitative section is based on basic statistical tools such as average, standard deviation and percentile. They are applied to the absolute errors and relatives errors.The Cylindrical Explosion (2D) study is purely qualitative. Errors are calculated as the difference between the given reference and obtained results.

The convergence study focuses on second order Lax-Friedrich (LXF) flux. This organization is presented in the following table;

Figure 1: Cylindrical Explosion, organization

The Forward facing step qualitative study is based on both HLLC and Rusanov fluxes associated with Bath & Jespersen and Venkatakrishnan limiters.
The same approach is conducted for the Double Mach reflection. A fifth-order Weno solver is added.

Computations have been performed via a given Fortran code.Minor modifications were performed on the code. The goal of the current study is to Validate the code and compare Riemann solvers in order to identify the one which gives the most conclusive result for each experiment. Limiters are taken into account being associated to Riemann solvers.

4   Results and Discussions

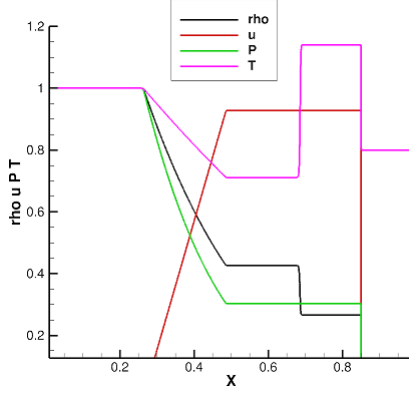## 4.1   1D-Cylindrical Explosion

4.1.1   Reference solution

Figure 2: Given numerical results, considered as reference in the current study. Physical features (rho, u, P and T) evolution over x are presented for t equals 0.2 secs.

Figure 2 represents the evolution of physical parameters (rho, u , P and T) in the shock tube. To ease the conversation with the reader, the above figure is divided into 5 regions of interests.
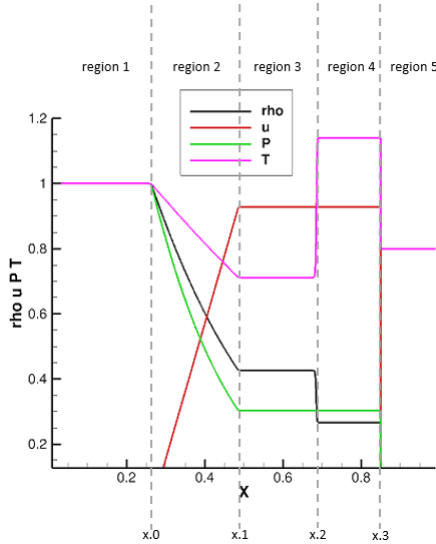

Figure 3: Given numerical results, divided into 5 regions

Region 2 is constrained by two points, respectively 'x.0' and 'x.1'. The region 2 depicts the position of a **rarefaction wave** moving to the left. Parameters properties are continuous in this region.

'x.0' and 'x.1' are the positions of the head and tail of the wave. At point 'x.2', P and u are continuous whereas rho and T do a discontinuous evolution. This phenomena is the physical meaning of a **contact discontinuity**[6]. At location 'x.3', all physical quantities are discontinuous. It highlights a **Shock wave** (moving to the right) which has zero-width transition.

Obtained computations using Lax-Friedrich Flux and reconstructions fluxes HLL and HLLC are compared to reference in the following paragraph.
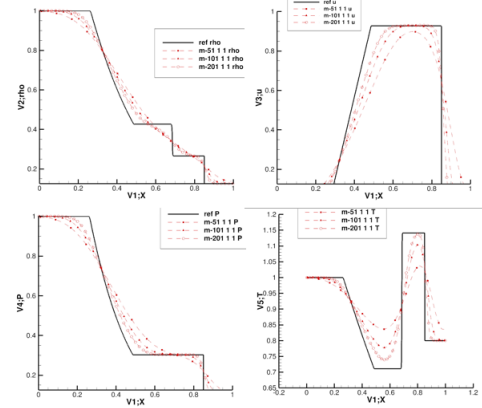
4.1.2   Comparison to Reference

Qualitative

Figure 4: Numerical results obtained via first order Lax-Friedrich Flux at time t=0.2. Computations performed on three meshes

Figure 4 represents the results obtained using first order Lax-Friedrich Flux on three meshes. Can be noticed that the rarefactions' endpoints are strongly rounded. The constant state making the transition between the rarefaction wave and the contact discontinuities is not accurately approached. The same phenomena is visible on the region between the contact discontinuities and the shock wave. The shock wave is predicted, however its evolution occupies a larger zone than the reference shows with sharp discontinuities. The scheme is diffusive. The spreading of the shock wave via numerical calculation is habitual [2].
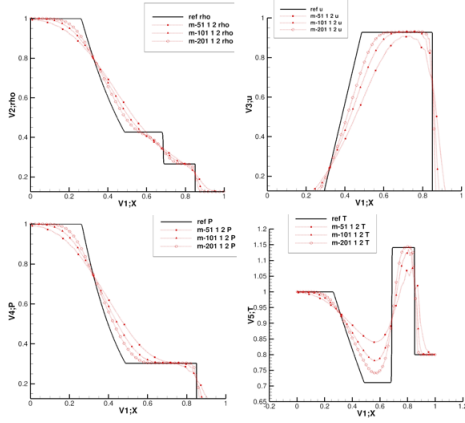
Figure 5: Numerical results obtained via second order Lax-Friedrich Flux at time t=0.2. Computations performed on three meshes. Physical features presented; rho,P, u and T

Figure 5 indicates physical properties calculated via Lax-Friedrich Flux with a second order. Results on three meshes are presented. The endpoints of the rarefaction wave are rounded in a lower proportion than LXF first order (Figure 4). Constant state are correctly predicted. Discontinuities are approached on a smaller zone. In term of temperature , a small overshoot is visible. Computations do not present oscillations in the vicinity of the contact discontinuity and shock wave which is positive (Figure 4). The method seems to have more difficulties approximating the contact discontinuities than the shock wave. This phenomena is explained in common and explained in [2],[6].
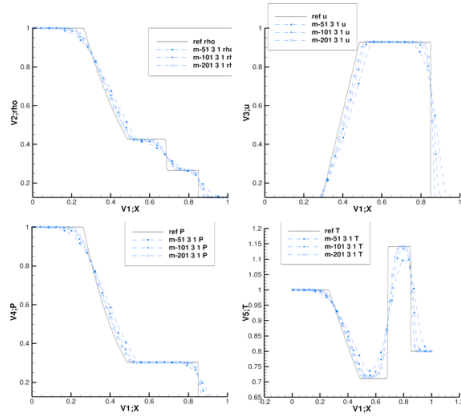

Figure 6: HLL, order 1

The above figure represents physical quantities obtained via HLL first order. The endpoints of the rarefaction are rounded but not as in (Figure 4). Constant states are poorly approached. Results in this field are improved in (Figure 7). Discontinu-

ities are not predicted on small areas. This phenomena was expected especially for the contact discontinuities. The HLL is known not being able to keep contact discontinuities sharp[6]. It can be explained by the fact that it ignores the middle wave representing the middle advection wave[6]. Globally results are graphically more accurate using the second order as it can be seen in (Figure 7).
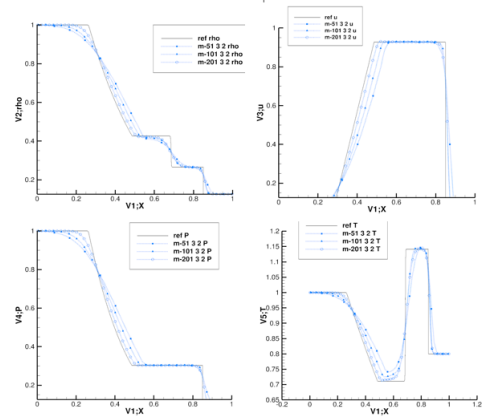
Figure 7: second order HLL. rho, p , u and T x evolution, three meshes

Figure 8 and Figure 9 represent respectively results given using HLLC first and second order. Obtained results are quite accurate. Rarefaction' endpoints are still rounded but constant state are properly approached. Contact and shock discontinuities are predicted on small zones which mean than contact and shock transition are sharper which better approach the reference and the physical expectation. In (Figure 9) a noticeable overshoot is visible for the temperature.

Figure 8: HLLC, order 1

Figure 9: HLL, order 2

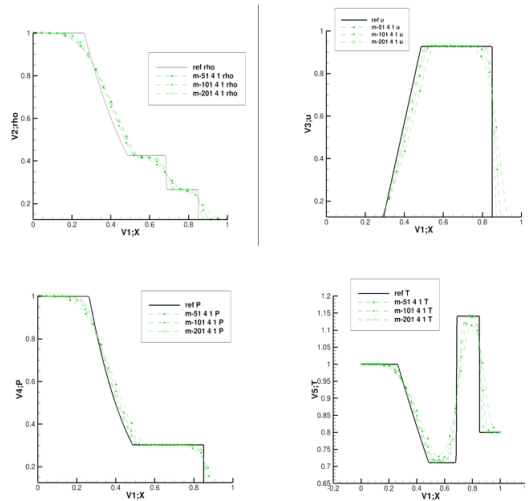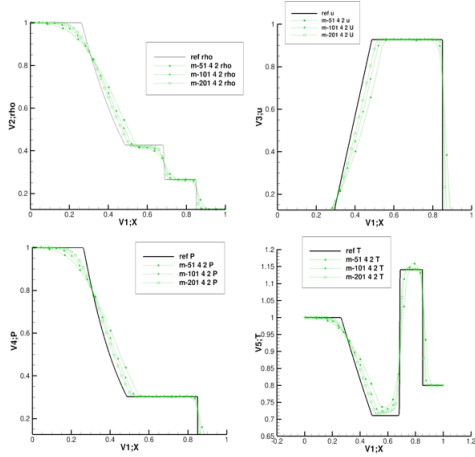Second order scheme give better results for all schemes. As the mesh increases results change. A quantitative approach will give more insight of the phenomena.

Plotting the internal energy is often accepted to discuss the quality of a solution[3]. The internal energy is given by

$$e = \frac{p}{((\gamma - 1)\rho)} \tag{21}$$

however in the current context, the pressure and density are close to zero. Because of the ratio, small errors will be exaggerated[6]. Consequently another statistical approach is used in the next paragraph.

quantitative Statistics are performed on results obtained on the finest mesh and second order fluxes. The feature studied is the density. The quantitative section is aiming to identify more accurately the flux which performs better in the current context.

	HLLC	HLL	LXF
σ	0.018957	0.019491	0.026606
gain(%)		2.737017	28.74778

Table 2: Standard deviation of the absolute errors calculated for HLLC, HLL and LXF. Fluxes are classified according to the Standard deviation value. As HLLC has the smallest standard deviation, it is positioned on the left. On the contrary LXF with the highest result on the right. The gain(%) represents the HLLC'gain compared to HLL and LXF.

In term of standard deviation of the absolute errors. HLLC obtains the most conclusive results and performs $\approx$ 2.7% better than HLL and $\approx$ 28.75% better than LXF. As seen graphically, HLLC and HLL do not differ significantly. Difference is more noticeable with LXF which stands aside. This phenomena is also visible in the next tables.

	HLLC	HLL	LXF
mean	0.014646	0.01549	0.025524
gain(%)		5.45037	42.61892

Table 3: Average value of absolute errors calculated for HLLC, HLL and LXF. HLLC's gain is also presented.

In term of average of absolute errors, the same fluxes ranking is depicted. HLLC gives the best results in both standard deviation and average. The coefficient of variation is not calculated as results from the standard deviation and the average are closed to zero. Nevertheless, can be admitted that HLLC performs better on dispersion indicators.

	HLLC	HLL	LXF
mean_relative_error	2.945817	3.195865	5.604864
gain(%)		7.82411	47.44178

Table 4: Average value of relative errors calculated for HLLC, HLL and LXF. HLLC's gain is also presented

	HLLC	HLL	LXF
percentile 75	4.3925	4.882444	8.640913
gain(%)		10.0348	49.16625

Table 5: Percentile 75 for HLLC, HLL and LXF. HLLC's gain is also presented

In term of relative error; The average of relative errors for HLLC is $\approx$ 2.3. Moreover, 75% of relatives errors are inferior or equals to 4.4%. Once again HLLC performs better than the other fluxes as it can be seen in the table above.

Discussion For all previous methods, positions of the waves are accurately predicted. It is due to the conservative character of Godunov method [3]. Positively, no entropy glitch are visible inside the rarefaction[6]. This phenomena is more likely to happen in sonic rarefaction[6]. The rarefaction wave is correctly approximated by all methods as it is a smooth flow features. Discrepancies appear at the head and tail of the wave. Results are globally satisfactory especially for the pressure. Results are in accordance with [3] and [6], hence the code is considered as Validated.

HLLC and HLL perfom better than Lax-Friedrich(LXF) fluxes in the current study. Graphical study does not allow to differentiate HLLC and HLL results. The statistical approach reveals better results from HLLC.

4.1.3 Convergence study, mesh refinement

We expect results in term of accuracy to get better as the mesh is refined[3]. The convergence study is focuses on the second order Lax-Friedrich Flux. Data used to perform these graphs are available in the appendixe.
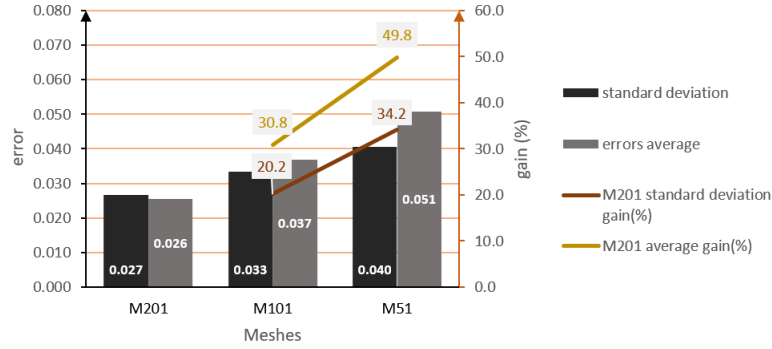

Figure 10: Second order Lax-Friedrich, 3 meshes. The standard deviation of the absolute error and the error average are presented for the three meshes. Meshes are classified according to their results. The finest mesh's gains compared to the other meshes are given.

In term of standard deviation, LXF performs better in the finest mesh; approximately 31 and 50 % than on the medium and coarse mesh.
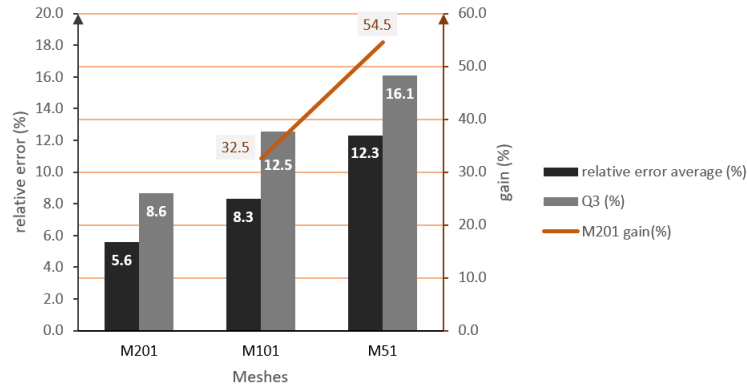

Figure 11: Second order Lax-Friedrich, 3 meshes. The average of absolute errors and Percentile 75. The gain(%) of Lax-Friedrich flux on mesh 2 in term of error average is presented

In term of relative error, LXF performs better in the finest mesh; approximately 32 and 54 % than on the medium and coarse mesh.
As expected, LXF performs better on the finest mesh.

4.1.4 Cylindrical Explosion

2D-Cylindrical Explosion

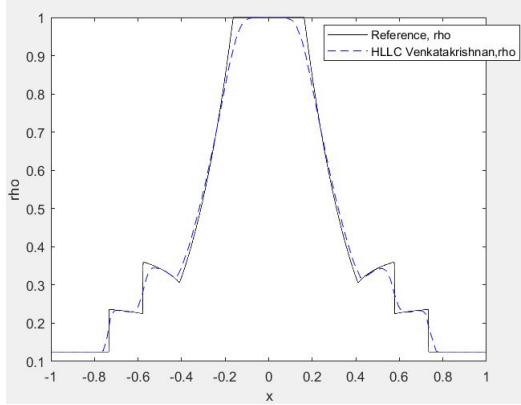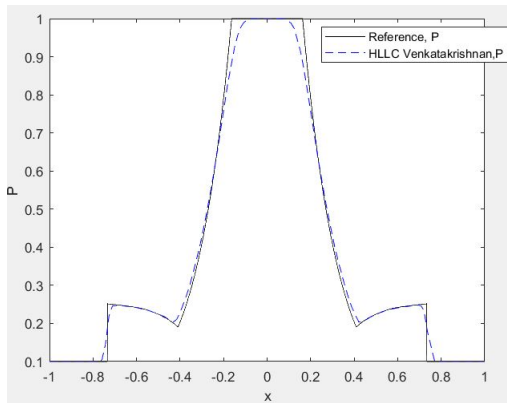Figure 12: HLLC Venkatakrishnan, rho

Figure 13: HLLC Venkatakrishnan,P

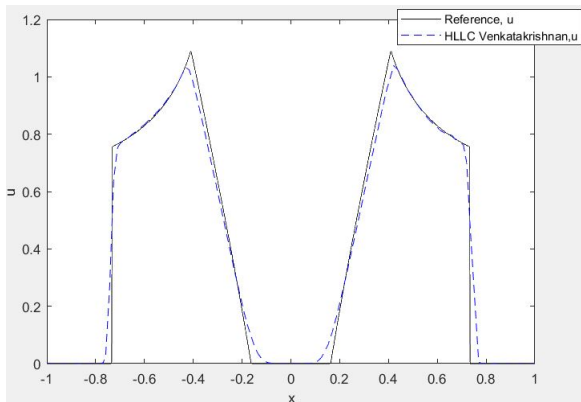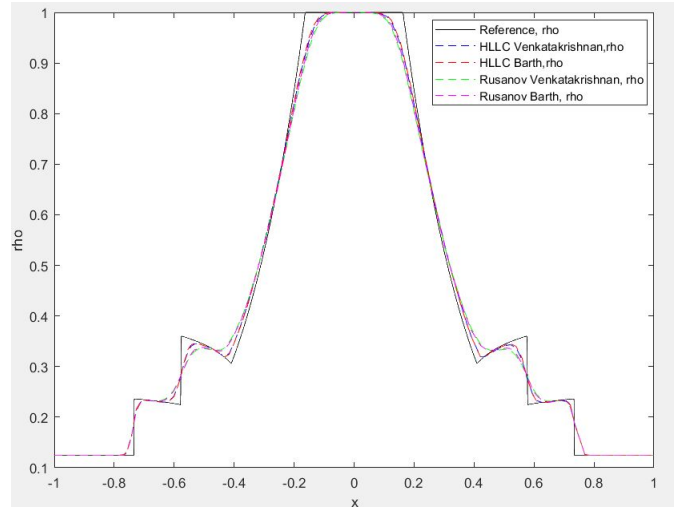
Figure 14: HLLC Venkatakrishnan,u

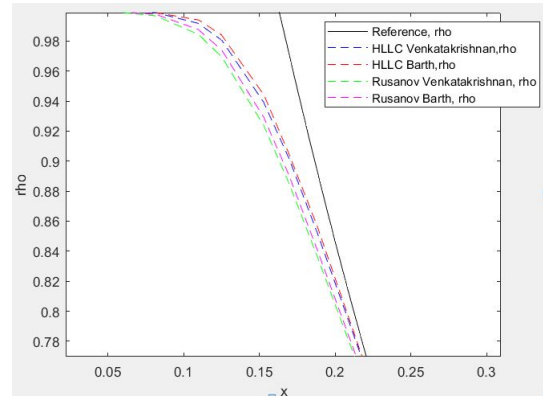Figure 15: rho, fluxes and limiters comparison

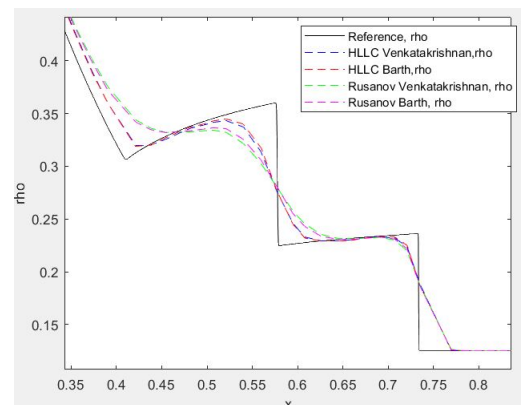Figure 16: rho, fluxes and limiters comparison, zoomed in

Figure 17: rho, fluxes and limiters comparison, zoomed in

Discussion Results are close to those obtained in 1D. Scheme ranking in term of global accuracy for fluxes stays the same. This similarity is not always "obvious": In [6] it is said that Scheme performing in 1 dimension does not necessarily give conclusive results for higher dimensions[6]. The 2D Experiment allows to distinguish limiters' influence. Barth & Jespersen predicts slightly more accurately physical features when associated to both fluxes.
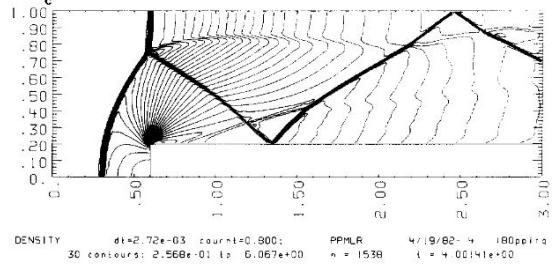
Reference

Figure 18: Reference PPMLR, density, 30 contours:0.2568-6.067

4.2 2D-Verify Implementation

4.2.1 Forward facing step

Description, overview The results present the evolution of density between time t equals to 0 and 4. At the start of the experiment, a shock wave forms in front of the step (Figure 19). The shock moves progressively away from the step and 'follows' a curved trajectory above the corner of the step. It strikes the upper wall at a time ≈ 0.7 and a location x ≈ 1 (Figure 20). The shock is reflected and moves downward.
As experiment goes on, the location of the point of reflection moves left (Figure 21). Meanwhile the reflected shock reaches the upper surface of the step.
The angle between the incident shock and the upper wall augments and reaches the maximum value for a regular reflection ($40° at \gamma = 1.4$). A Mach stem forms (Figure 22).The location of strike one reaches the location x≈ 0.75.
The location of the strike 2 moves left. The second reflected shock propagates toward the grid and reaches the top right corner (Figure 22).The location of the second strike reaches the position x≈ 1.6 at time ≈ 2.5.A second mach stem forms (Figure 23).The second reflected shock strikes the upper wall. A third reflected shock is generated (Figure 24). The location of the third strike moves left (Figure 25).

The reference results give narrow shocks. The bow shock is slightly wider as its base and get thinner as it moves above the corner.The Mach Stem is positioned at x≈ 0.6 and is 25 units long. The reflect shock reaches the upper surface of the step at x≈ 1.35. The second reflected shock strikes the upper wall at x≈ 2.4.
Both contact discontinuities are sharp. A weak shock originating from the corner of the step is clearly visible and is being refracted by the second reflected shock. Instability near the bottom wall are small.
Can be noticed that contact discontinuities are more smeared than shocks. It seems that this phenomena is common in the field [2]. Smearing may be reduced by the use of higher order of accuracy[2]. Methods exist to improve these results.[5]
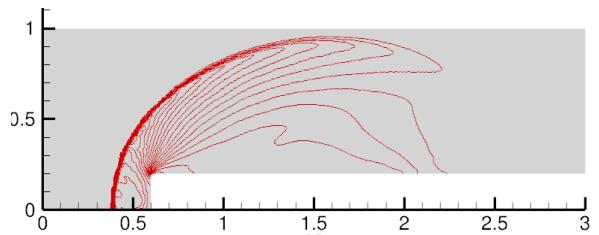
HLLC, Venkatakrishnan

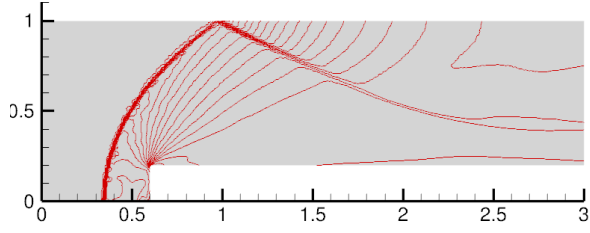Figure 19: Forward facing step, HLLC, Venka, 30 contour:0.2365-5.647 t=0.517059

15

Figure 20: Forward facing step, HLLC, Venkatakrishnan, 30 contours:0.2628-7.564 t=1.00044

Figure 21: Forward facing step, HLLC, Venkatakrishnan, 30 contours:0.2805-7.717 t=1.50285

Figure 22: Forward facing step, HLLC, Venkatakrishnan, 30 contours:0.2669-6.650 t=2.01716
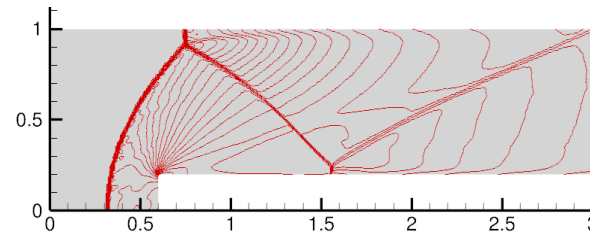
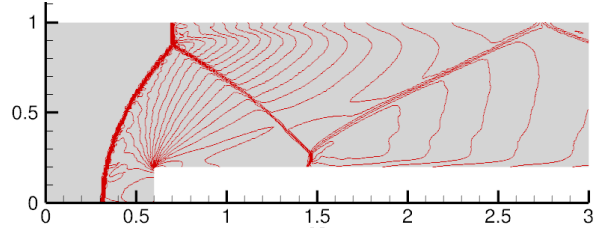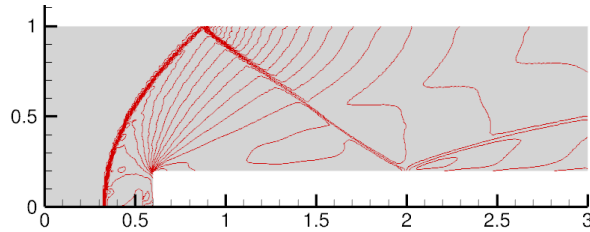Figure 23: Forward facing step, HLLC, Venkatakrishnan, 30 contours:0.2688-6.602 t=2.50107

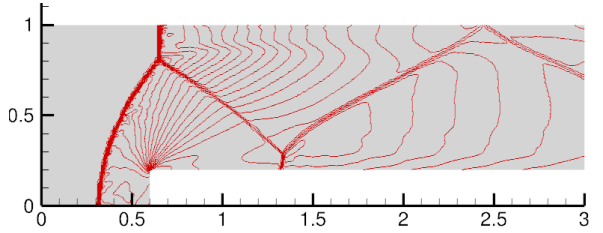Figure 24: Forward facing step, HLLC, Venkatakrishnan, 30 contours:0.2673-6.383 t=3.00018

Figure 25: Forward facing step, HLLC, Venkatakrishnan, 30 contours:0.2568-6.067 t=4.00141

Figure 25; The general position and shape of the different shocks is in correct accordance with reference's data. However, shocks width are larger in the computation and suffer from pre and post shock oscillations. This phenomena is particularly visible on the bow shock, the first reflected shock and behind the mach stem. The weak oblique shock is not resolved and a Mach stem is visible at a position x=1.35 whereas it is not in the reference. The contact discontinuities originating from the triple point is spread somewhat. Hence, the contact discontinuities is not as visible as the one in the reference and vanishes before the second reflected shock. The effects of boundary layer on the upper surface of the step generate more perturbations than in the reference.
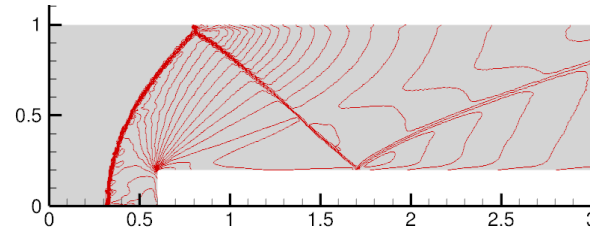
HLLC, Barth

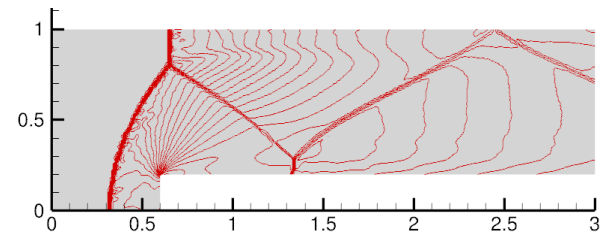Figure 26: Forward facing step,HLLC, Barth, 30 contours: t=4

Figure 26; results are almost identical to HLLC, Venkatakrishnan
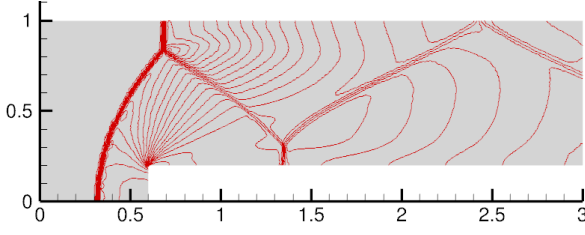
16

Rusanov, Venkatakrishnan

Figure 27: Forward facing step, Rusanov, Venkatakrishnan, 30 contours: t=4

Figure 27; the shocks' shape and position are acceptable. Results are less accurate than HLLC, Venka (Figure 25). The shocks' width are also larger. Pre and post shocks' oscillations degrade result in the same extent as in (Figure 25). Behind the upper Mach stem, less perturbations are noticed. The oblique shock is not resolved and the Mach stem is visible. Contact discontinuities are drastically smeared. The effects caused by boundary layers along the upper surface of the step are very weak.
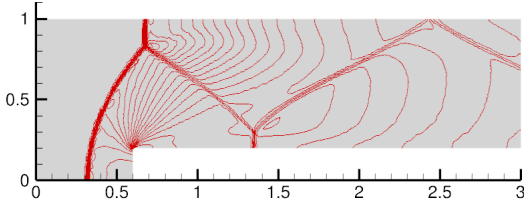
Rusanov, Barth

Figure 28: Forward facing step, Rusanov, Barth, 30 contours: t=4

Figure 28; results are almost identical to Rusanov, Venkatakrishnan.

Discussion HLLC gives better results. The current study does not allow to distinguish results from both limiters. Fluxes used show difficulties evaluating the Mach stem. According to [6], the Mach stem phenomenon is linked to the smearing of the shock: if the shock is smeared to a large extent, the Mach stem is predicted late and does not reach the correct position. The opposite statement for small smearing is right[6]. In the paper[6], the same difficulty of predicting the Mach stem is encountered by The MacCormack and Godunov schemes. It is also said that predicting properly the Mach stem would require an "impractically large number of zones"[6].

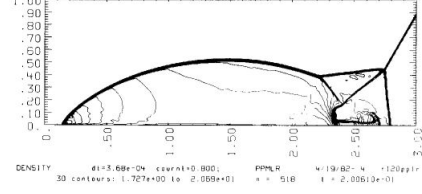### 4.2.2 Double mach reflection, Results and Discussion

Reference

Figure 29: Reference

The above results from [6] show the density contours in the domain restricted to x ∈ [0, 3] at time t equals 0.2. Results highlight two Mach stems and two contact discontinuities. In the paper [6] the second contact discontinuity is said to be weak. The second Mach stem almost disappears before reaching the contact discontinuities resulting from the first Mach reflection.

Shocks are represented as narrow and don't suffer from 'pre or post oscillatory' behaviors. The treatment of oscillations have impacted negatively the width of the shocks[6]. However such drawbacks do not impact significantly the accuracy of the results. The jet phenomena depicted in the area bounded by the second mach shock, the reflected shock and the reflecting wall is sharp, clearly visible and considered as particularly "well represented"[6].

In the paper[6], the presented scheme is considered as particularly efficient on the current study and has overcome difficulties. Numerical scheme have difficulties evaluating accurately the density evolution of the second Mach shock, more specifically its weakening as it reaches the contact discontinuity. Moreover the formation of the jet is considered to be difficult to compute[6].
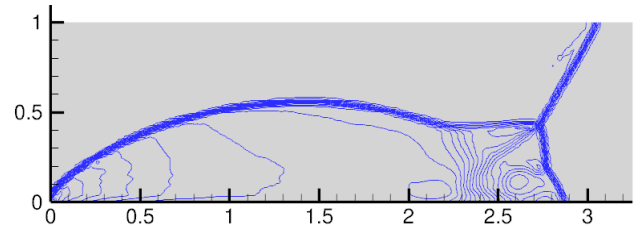
HLLC
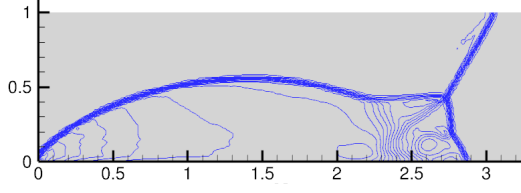

Figure 30: HLLC, Venkatakrishnan

Figure 31: HLLC, Barth Jespersen

Both results computed via Venkatakrishnan and Barth Jespersen are really similar. General shape and position of the different phenomena are not properly identified. Shocks' width are larger than in those in the reference. Spurious oscillations are noticeable and degrade shocks' quality. Mach stem are poorly approximated. In a lower extend this phenomena has been noticed with ETBFCT[6]. It is attributed to the poor resolution of the jet. The contact discontinuity at the origin of the jet is smeared. Nonphysical structures around the three-shocks interactions are visible. This behavior is noticed in [6] (Fig 9b) for the MacCormack's method. The weak shock is broader than expected.
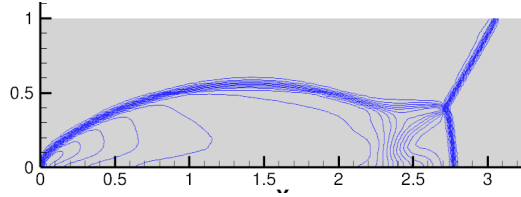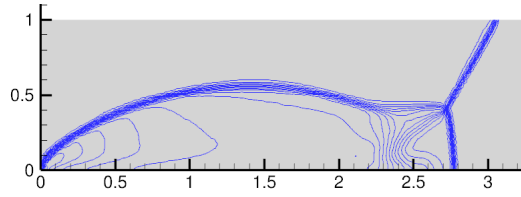
Rusanov

Figure 32: Rusanov,Venkatakrishnan

Figure 33: Rusanov,Barth Jespersen

Above results obtained using Rusanov with Venkatakrishnan and Barth are close to each other. Overall results are not acceptable. Shocks are poorly described and suffer form oscillations. Jet structures are not resolved. The shape of the Mach stem 1 is more realistic than obtained via HLLC. Nevertheless, results are not as conclusive as those obtained via HLLC.
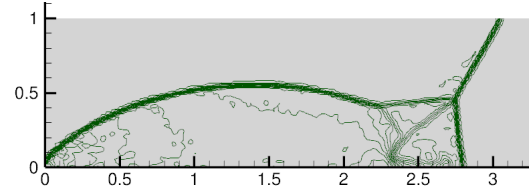
Weno

Figure 34: Weno

Results obtained by WENO predict more accurately the position and width of shock than MUSCL scheme. Monotonicity seems preserved. Good results were expected as Weno is often considered to be suitable for experiments which include shocks and smooth structure[2]. Some spurious oscillations are visible. Weno scheme used 'alone' is not always monotonicity preserving [2]. In the of [2], researchers have linked fifth order Weno to Runge-Kutta scheme[1] . In their study, results were non oscillatory at a CFL equals to 0.2 but oscillatory at CFT equals 0.4. The Runge-Kutta 'extension' and tests conducted at different CFL number could represent a future work for the current assignment. Moreover "starting error" appears as in ETBFCT [6] and unphysical physical element under the reflected shock. These phenomena are noticeable in the above result. Can be pointed out that high order Weno schemes suffered from computational cost.

5 Conclusion

The Cylindrical explosion experiment has revealed a correct prediction of constant states by Lax-Friedrich, HLL and HLLC. The shocks' position are appropriately predicted. Contact discontinuities represent more difficulties at being approximated than shocks. The different fluxes show deficiencies at evaluating the head and tail of the rarefaction wave. HLLC and HLL perform better than Lax-Friedrich. Can be pointed out that HLL indicates weaknesses at maintaining contact discontinuities sharp as expected. On the contrary HLLC gives conclusive results at approximating contact and shock transitions. HLLC can be considered as the best proposal on the current study for this 1D Experiment. A grid convergence study has been performed on Lax-Friedrich and results are in accordance with theory.
In 2 dimensions, same fluxes ranking is obtained. The added dimension has provided information on limiters' performances. Barth & Jespersen gives more convincing results than those obtained via Venkatakrishnan. This observation applies to both HLLC and Rusanov fluxes.
As obtained phenomena coincide with papers' results, the code is considered as Validated.

The Forward facing step has distinguishes HLLC and Rusanov accuracies. Rusanov associated to Venkatakrishnan does not suggest appropriated shocks' position. Contact discontinuities are drastically smeared. Oscillations deteriorate overall results.
HLLC seems more appropriated and gives conclusive results in term of shocks' positions. However shocks are larger and suffer from oscillations.
Both fluxes haves difficulties predicting the Mach Stem as it was expected in the paper. Overall results are in accordance with those from [6]. The code is considered as validated.

The Double Mach reflection has highlighted HLLC's difficulties. Fifth order Weno gives conclusive results in term of Monotonicity. Obtained results are coherent with [6] despite some non physical features. The code is validated.

The different experiments have emphasised on fluxes' strengths and weaknesses. To continue the study, more sever problem could be used such as the Blast Wave introduced by Woodward & Collela.

6 References

References

[1] Chi-Wang Shu bernardo Cockburn. "Runge-Kutta Discontinuous Galerkin Methods for Convection Dominated Problems". In: (2001).

[2] Chi-Wang Shu Dinshaw S Balsara. "Monotonicity Preserving Weighted Essentially Non-oscillatory Schemes with Increasingly High Order of Accuracy". In: (1999).

[3] Eleuterio F.Toro. *Riemann Solvers and Numerical Methods for Fluid Dynamics*. Springer, 1997.

[4] Nancy Hall, ed. *Normal Shock wave equations*. National Aeronautics and Space Administration. 2018. URL: https://www.grc.nasa.gov/www/k-12/airplane/normal.html.

[5] A Harten. "ENO schemes with subcell resolution". In: (1983).

[6] Philip COLELLA Paul WOODWARD. "The Numerical Simulation of Two-Dimensional Fluid Flow with Strong Shocks". In: (1983).

[7] GARY A SOD. "A Survey of Several Finite Differnce Methods for Systems of Nonlinear Hyperbolic Conservation Laws". In: (1977).

7 Appendices

7.0.1 Comment on the convergence of the solution has the mesh is refined

LXF Quantitative

standard deviation

	M201	M101	M51
errors average	0.0255	0.0369	0.0508
standard deviation	0.0266	0.0334	0.0404
M201 standard deviation gain(%)		20.2400	34.2129
M201 average gain(%)		30.8298	49.7760

percentile

	M201	M101	M51
Q3 (%)	8.64091285	12.53911274	16.09018763
relative error average (%)	5.60486395	8.30623811	12.32575791
M201 gain(%)		32.61073130	54.52722673